IIETA International Information and Engineering Technology Association
Advancing the World of Information and Engineering

Mathematical Modelling of Engineering Problems
Vol. 9, No. 4, August, 2022, pp. 955-963
Journal homepage: http://iieta.org/journals/mmep

Dynamic Modelling of Docking Autonomous PODs in Tandem Configuration

Osama M. Al-Habahbeh*, Romil S. Al-Adwan

Mechatronics Engineering Department, School of Engineering, The University of Jordan, Amman 11942, Jordan

Corresponding Author Email: o.habahbeh@ju.edu.jo

https://doi.org/10.18280/mmep.090412

Received: 4 May 2022
Accepted: 11 August 2022

Keywords:
autonomous PODs, autonomous transportation, FEA simulation, merging speed, POD vehicles, tandem docking, transportation design

ABSTRACT

An adaptable transportation concept is proposed; comprising a fleet of autonomous PODs that can merge and separate based on passengers' demand. The purpose is to match the number of seats with the number of passengers, thereby reducing vehicle size and energy consumption. It enables passengers' in-person communication and simultaneous arrival. Since each POD has its own motor, if full power is not needed, one of the motors can be turned-off to save energy. The merging process is investigated so as to find the safe docking speeds when two PODs merge in tandem configuration. If the docking is not done at the right speed, it may cause damage to the vehicle, or else be inefficiently slow. The PODs are represented by finite element models, which are simulated to determine the safe merging speeds. The speeds are determined for different docking scenarios and POD materials; ranging from 1.4-16 km/h. The safe speeds depend on the type of material and adopted damage criterion; Nonmetallic materials showed higher tolerance than metallic materials in response to docking impact. As a recommendation for future work, other materials and configurations can be investigated, and the effect of the proposed system on traffic conditions can be evaluated.

1. INTRODUCTION

Autonomous vehicles are disrupting transportation systems in many countries. However, in terms of design, most of these vehicles are similar to ordinary vehicles, especially when it comes to the rigid passenger capacity. On the other hand, a vehicle that can accommodate only one person is called a POD. In the traditional case, the passenger onboard the POD should be driving, but in the autonomous case, this person can be just a passenger. The use of autonomous PODs can be a good way to save cost, both in fuel and space. This is when only one person wants a ride. However, when two or more people need a ride, they should use a traditional-looking autonomous vehicle or ride PODs individually. The problem with the traditional-looking autonomous vehicle is that most of the time there are vacant seats. Which is reflected in additional cost. As for riding PODs individually, it doesn't allow direct interaction between the passengers. Moreover, it can't guarantee that they depart together and arrive together. Therefore, a possible solution is to design these PODs in such a way that they can stick together when needed, and detach when needed.

Autonomous POD vehicles are poised to become an important part of future transportation landscape. Therefore, studying the safety of their operation is essential. Several patents [1-7] have shown that POD vehicles can merge and separate as part of their operation. During the joining process of the two PODs, unwanted collisions or impacts could happen; If the impact speed is high enough, it may cause damage in the body of the vehicle. On the other hand, if the impact is avoided by making the approach speed too low, it will make the PODs' joining process inefficiently slow.

Therefore, it is required to investigate the optimum speed for joining the two POD vehicles. This work focuses on finding the optimum velocity for merging two autonomous PODs in tandem configuration. Driving and impact characteristics of multiple autonomous vehicles were modeled by Zong et al. [8]. Xia et al. [9] presented a novel controller for autonomous vehicles which offers less errors and faster speed. A call for the meteorological and the transportation communities to enhance the safety of autonomous vehicles was reported by Walker et al. [10]. Chen et al. [11] explored the mechanism of crashes involving autonomous vehicles. Malik et al. [12] carried out an experimental study of denial of service attacks against platoon of smart vehicles. Chen et al. [13] developed an artificial intelligence inverse problem solution for traffic collision reconstruction. Tho et al. [14] proposed a motion planning method based on minimum distance for lane change of autonomous vehicles.

He et al. [15] proposed a novel emergency steering strategy based on hierarchical control architecture. It was hypothesized by Jin et al. [16] that the occupant will be more protected using rotational seat to alter orientation according to impact direction. Lee and Kum [17] proposed a collision avoidance system to evaluate risks associated with surrounding vehicles. Corso et al. [18] implemented adaptive stress testing and encoding relevant information to identify failure scenarios of autonomous vehicles. Xu et al. [19] investigated the characteristics of crashes involving connected autonomous vehicles. Dlugosch et al. [20] tested metal-reinforced composite materials under dynamic axial loading. Müller et al. [21] adopted a material model to generate a material database for three hardwood species. While Yusof et al. [22] introduced a hybrid design approach to develop a conceptual design of oil

palm polymer crash box. Abdullah et al. [23] conducted an extensive literature survey pertaining to crash boxes. Chen et al. [24] developed a multi-material design of a vehicle body considering both crashworthiness and social effects. Saenz-Dominguez et al. [25] analyzed the feasibility of honeycomb-like crash-box based on building block.

Liu et al. [26] explored the impact response of carbon fiber reinforced plastic tubes and aluminum tubes subjected to axial impacts. The effect of failure criteria of B-pillar on the accuracy of impact simulations was evaluated by Öztürk et al. [27]. Song et al. [28] used data from California automated vehicle collision reports to learn how to develop test scenarios. Oztürk et al. [29] developed an accelerated design method for a side door pillar to absorb crash energy. For the purpose of optimizing the vehicle design for crashworthiness, Yu et al. [30] used blank structures in the front-end of electric vehicles, whereas Noorsumar et al. [31] reviewed mathematical modeling of vehicle crash. Safety requirements of EVs were reviewed by Chombo et al. [32]. In order to improve the vehicle crashworthiness in frontal impact, an optimization process using optimal Latin hypercube design and response surface method was proposed by Liu et al. [33]. Gungor et al. [34] developed a control strategy for platooning a fleet of Autonomous Trucks; the main purpose of connecting the trucks is that they can arrive at the destination simultaneously. Al-Mamany [35] suggested improvements to the mobility demand management of High Occupancy vehicle lanes in two Indian expressways; this is an example of conventional solutions that can be used to reduce pollution and increase passenger comfort. By contrast, this work presents an unconventional way to achieve the same goals; by connecting the PODs, several benefits can be obtained:

1) Passengers can communicate directly and naturally.

2) If the road condition permits, one or more motors can be turned-off to save energy.

3) The passengers will arrive at the destination simultaneously.

4) No seats will be left vacant, which results in reducing energy consumption and road space needed.

Ulrich et al. [36] introduced operating strategies for a new modular autonomous vehicle; the vehicle comprises a drive unit and interchangeable capsule. Nonetheless, although it is a good idea, the process of capsule replacement needs additional equipment, power and time, which renders it impractical. Whereas the transportation system proposed in this work consists of a fleet of PODs that are capable of joining each other based on demand. The proposed PODs attachment process is practical because it requires no additional equipment and can be conducted quickly with minimum power. The main focus of this work is to study the merging process of two PODs in tandem configuration and investigate the impact safety during this operation.

2. PODs MERGING METHOD

The proposed smart transportation system consists of POD units as shown in Figures 1 and Figure 2, where the POD is the basic building block of this system. Figure 1 shows two separated POD vehicles and Figure 2 shows the PODs after joining each other in a Tandem configuration. The attachment process is done using Hitching Ports as shown in Figure 1. Once the PODs join each other, the windows can be opened so that the passengers can interact naturally. Since these vehicles will merge and separate based on passengers' demand, during the merging operation, unwanted collisions could take place. If the impact speed is too high, it could cause damage in the body of the vehicle. This work deals with this issue by using Finite element analysis (*FEA*) to model different POD merging conditions. As a result of the models simulations, the safe impact velocities during docking are determined based on material failure criteria. Some of the variables considered in this work include body material, panel thickness and absorbed energy. Without the knowledge of these speeds, either high or low velocities will be used. In such cases the high speed will cause damage and the low speed will cause delay.

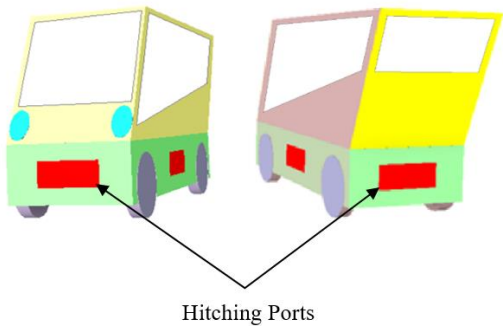

Figure 1. Front and back views of the Autonomous POD

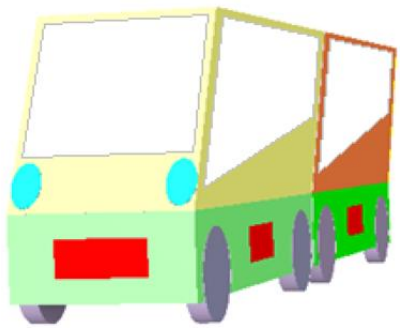

Figure 2. Two PODs docking in Tandem configuration

Each POD will have the ability to join other PODs and separate from them based on demand. The process starts when the passenger requests a ride using his smart phone. The request is received by a central control room (*CCR*). The *CCR* processes the request by contacting the nearest PODs; where the number of contacted PODs matches the requested number of seats (number of passengers). These PODs are commanded to move to the customer's location. The PODs arrive at the passenger's location, merge together to form a vehicle with seating capacity matching the number of passengers. The new vehicle picks up the customers and takes them to their destination. The cycle will be repeated as soon as new requests are received by the *CCR*. An essential part of the proposed transportation system is the PODs merging process. This work investigates the process of merging two PODs in tandem configuration. This scenario applies if two passengers requested a ride, or as part of a larger POD merging process to accommodate more passengers. The PODs merging process is simulated using two FEA models, as shown in Figure 1. The two models are joined in tandem configuration as shown in Figure 2. The dimensions of the POD are 1 m width × 1.5 m height × 3 m length. These measurements provide comfortable seating for one passenger and his belongings. The PODs

joining process will be done by attaching the corresponding hitching ports of each POD, as shown in Figure 1, Figure 2, and Figure 3. When two passengers request a ride, two PODs will move to the customers' location. They will merge together and form a tandem vehicle, as shown in Figure 2 and Figure 3. The merging process is done automatically where one of the PODs is parking while the other approaches it from behind. During the merging process, a sensitive parameter is the relative speed between the two joining PODs, as well as the impact angle. If the relative speed is low, the joining process will take longer time, which will increase the operational cost. On the other hand, if the speed is high, the impact during attachment may cause damage in the vehicle. Hence, it is necessary to find the optimum approach speed, which is the fastest speed that does not cause any failure in the PODs.

The POD models shown in Figure 1 and Figure 2 will be imported into FEA software, then used to simulate the joining process. For the POD's body, different materials will be investigated. These materials include metals and composites. In addition, different thicknesses of the outer body will be simulated. An additional variable is the angle of impact (AI). The impact velocity will be varied so as to find the optimum value for each set of conditions. In this kind of analysis, it is imperative to decide on the type of failure criterion to be used. Of course this depends on the type of the body material. The geometric modeling is done using SpaceClaim™ and the FEA simulation is done using ANSYS™. During PODs attachment, the loads on the deformed parts of the bodies are [37]:

$$\sum F_1 = m_1 a_1 \tag{1}$$

$$\sum F_2 = m_2 a_2 \tag{2}$$

Since m_1=m_2;

$$\frac{\sum F_1}{a_1} = \frac{\sum F_2}{a_2} \tag{3}$$

where, F_1 is the load on POD_1, which could originate from POD_1 motor power or the impact during merging; F_2 is the load on POD_2, which could originate from POD_2 motor power or the impact during merging; m_1 and m_2 are the masses of POD_1 and POD_2, respectively; a_1 and a_2 are the accelerations of POD_1 and POD_2, respectively.

During the attachment process, POD_1 will be parking while POD_2 will be moving and approaching POD_1 from behind. Using the work and energy principle, the energy balance during impact can be written as:

$$(T_1 + T_2)_i + U_{i-f} = (T_1 + T_2)_f \tag{4}$$

where, T_1 is the kinetic energy of POD_1; T_2 is the kinetic energy of POD_2; Subscripts i and f are initial and final states, respectively (before and after impact); U is the work done during impact.

The impulse-momentum theorem can be applied on the merging impact such that:

$$(m_1 v_1 + m_2 v_2)_i + \int_{t_i}^{t_f} F_1 dt + \int_{t_i}^{t_f} F_2 dt = (m_1 v_1 + m_2 v_2)_f \tag{5}$$

where, v_1 is the speed of POD_1; v_2 is the speed of POD_2.

By substituting m instead of m_1 and m_2, and removing F_1 because POD_1 is parking during the impact. Eq. (5) becomes:

$$m(v_1 + v_2)_i + \int_{t_i}^{t_f} F_2 dt = m(v_1 + v_2)_f \tag{6}$$

Mechanical stresses will develop in the contacting parts of the two PODs because of the above forces. The amount of stress can be written as:

$$\sigma = \frac{F}{A} \tag{7}$$

where, F is the impact force; A is the affected area.

The current analysis investigates the behavior of the structure assuming multiple materials. The materials used and their properties are listed in Table 1.

Table 1. Properties of materials used in the analysis

Type of material	Yield strength (MPa)
Steel 4340	470
AL 1060-H12	61
Composite-Epoxy glass fiber	440
Plastic-ABS high impact	27.4

3. MERGING SIMULATION RESULTS

The joining scenario into tandem configuration is simulated using FEA models of POD_1 and POD_2. A new combined tandem vehicle will be formed after the merger, as shown in Figure 2. There are two possible conditions that could happen during the merger; the first condition is when the two PODs are aligned accurately as shown in Figure 3. This is called central impact. In this situation, the AI will equal zero, as shown in Figure 3. The second condition is when the two vehicles are not perfectly aligned during the merger, as shown in Figure 6. This is called eccentric impact. In this situation, AI will be nonzero. In this work, a value of AI=20° is used to investigate this condition. The results of the two conditions are shown in Figure 4. These results correspond to a 1 mm panel thickness, 7 km/h impact velocity (*IV*), and body panel made of Steel 4340. The Yield Strength (*Y*) of this material equals *470 MPa*. In Figure 4, it is clear that the load at AI=20° is more critical than the AI=0 case. Therefore, the more critical case will be used for all subsequent work.

3.1 Central impact (AI=0°)

This condition is shown in Figure 3. During the docking process, impact force will affect the two corresponding sides of POD_1 and POD_2. Figure 3 shows the deformation resulting from this force. In Figure 4, it is clear that at AI=0°, the stress is lower than the AI=20° case. Hence, further work will focus on the more critical case which is AI=20° (Eccentric Impact). Figure 5 shows the impact energy behavior during docking; this figure demonstrates that internal energy increases during docking. In the same figure, kinetic energy decreases during docking as expected.

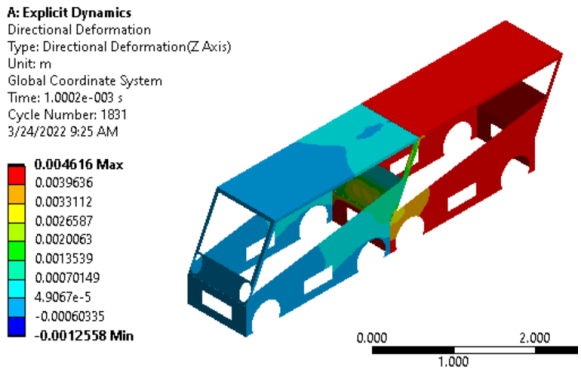

Figure 3. Tandem docking PODs at AI=0°

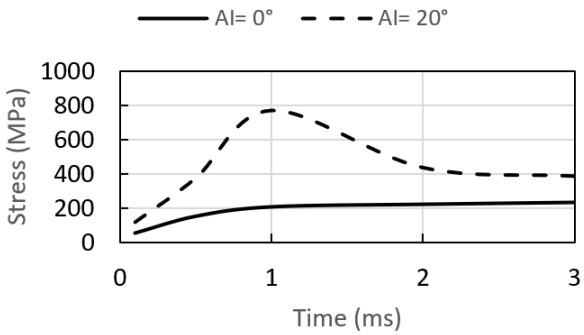

Figure 4. Equivalent stress for the two merging conditions

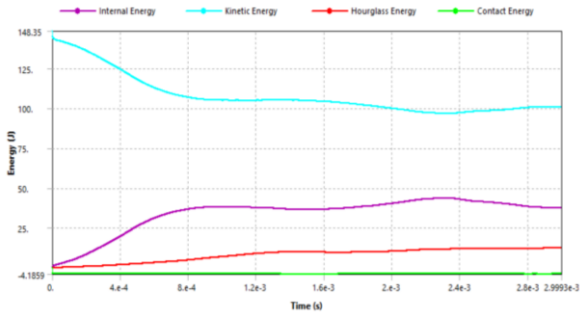

Figure 5. Energy summary during tandem docking

3.2 Eccentric impact (AI=20°)

This condition is illustrated in Figure 6, where POD_2 is trying to merge with POD_1 by approaching it from behind. However, the process is not going well due to some condition such as wind, uneven road, sensor error, etc. This scenario assumes that the angle between the two PODs is 20°. This will make the front edges of POD_2 bump into the aft side of POD_1, as shown in Figure 6. The stress distribution shows that the maximum value occurs near the center of the aft side of POD_1. This scenario is more critical than the central impact case. Therefore, it will be investigated further. The parameters used in this case are the same ones used in the previous case (Central impact), where *IV* is *7 km/h* and panel material is Steel 4340, with thickness of 1 mm.

For this scenario, the velocities for two impact speeds are plotted in Figure 7; approximately, the peak of the impact occurs after 1 ms. The variation of acceleration for two impact speeds is shown in Figure 8; it reflects the acceleration at the beginning followed by deceleration due to the docking impact. These results are based on a body panel made of Steel 4340 with thickness=1 mm. The yield strength (*Y*) of this material is *470 MPa*, as shown in Table 1. The deformation of the body panel during impact for two velocities is shown in Figure 9, for the same previous conditions. It is noticed that the deformation increases with time and impact velocity.

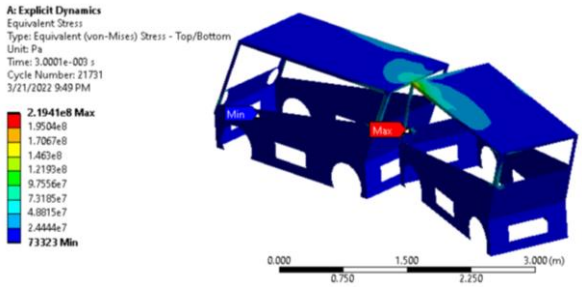

Figure 6. POD_2 approaching POD_1 at AI=20°

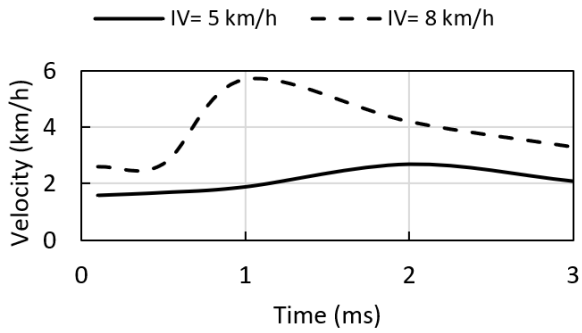

Figure 7. Velocity during docking impact

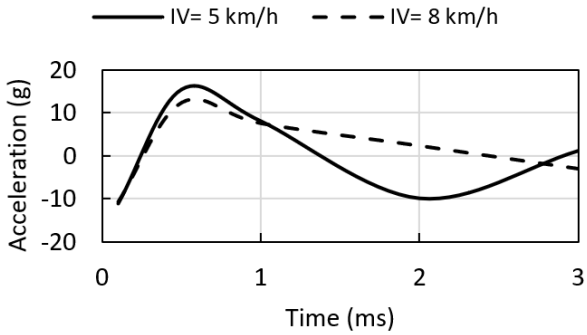

Figure 8. Acceleration during docking impact

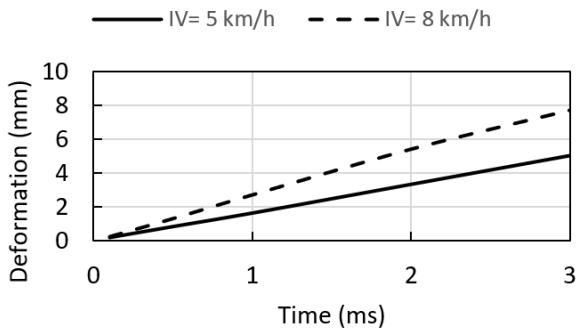

Figure 9. Body panel deformation during impact

The docking impact force is shown in Figure 10 for two velocities. The figure is based on steel 4340 panel with 1 mm thickness. The behavior is highly dependent on the velocity. Figure 11 illustrates the impact energy for steel 4340 with

panel thickness of 1 mm. It shows the variation for two velocities. It is noticed that the impact energy is maximum at the beginning of the impact, then it decreases with time. Figure 12 shows the stress-strain curve for Steel 4340 body panel, with thickness of 1 mm and *IV* of *8 km/h*. The Yield point at 470 *MPa* is not clear on the curve. It is noted that the curve does not look like a traditional tensile test curve; the reason is that the nature of the impact is more complicated and involves different loading and design conditions. Stress versus *IV* for Steel 4340 is shown in Figure 13, where the panel thickness is 1 mm. It is noticed that the relationship is nonlinearly proportional. Strain versus *IV* for Steel 4340 is shown in Figure 14, where the panel thickness is 1 mm as well. For the same material and panel thickness, Figure 15 shows the deformation variation with *IV*, where the relationship is nonlinear proportional.

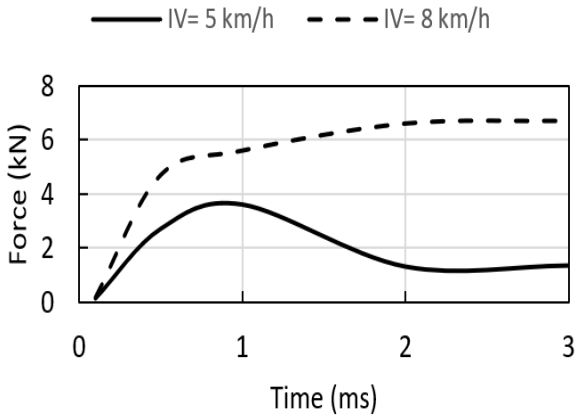

Figure 10. Impact force on body panel

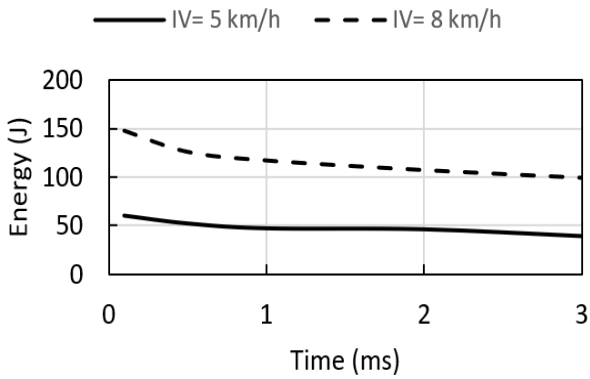

Figure 11. Impact energy for Steel 4340 body panel

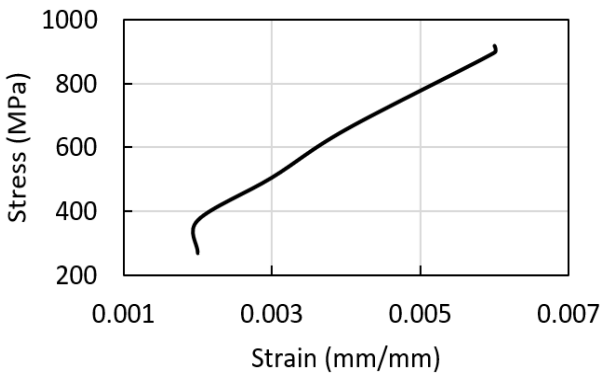

Figure 12. Stress-Strain curve for Steel 4340 body panel

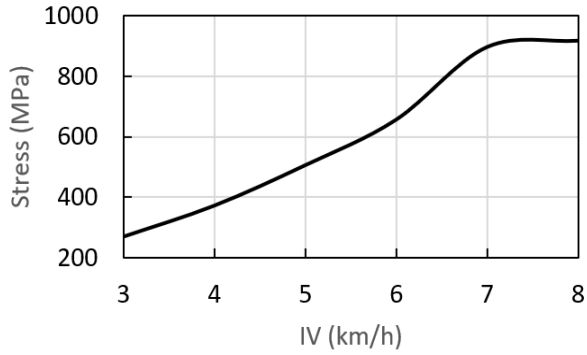

Figure 13. Stress variation with *IV* for Steel 4340

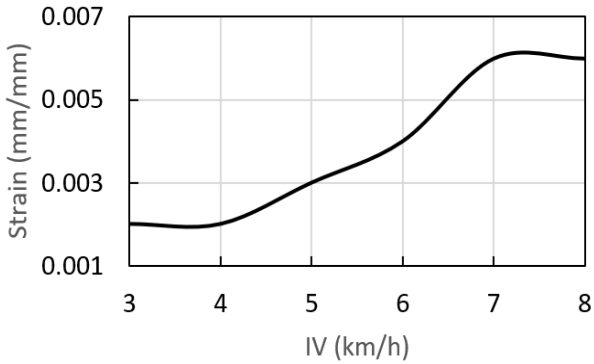

Figure 14. Strain variation with *IV* for Steel 4340

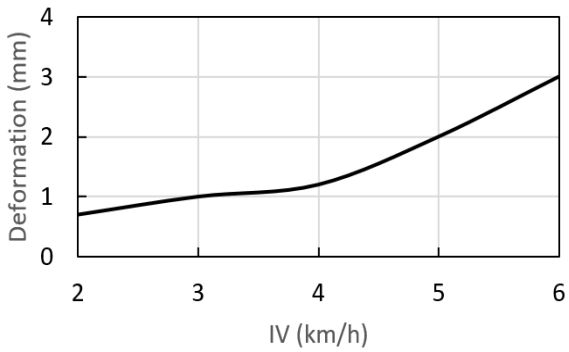

Figure 15. Deformation variation with *IV* for Steel 4340

3.2.1 Effect of body panel thickness

The stress variation with thickness for Steel 4340 is shown in Figure 16. The relationship is nonlinear and inversely proportional. As the body panel gets thicker, the stress goes down, but not linearly. This curve is based on 5 *km/h IV* and 20° AI. This means we can use more speed if we make the panel thicker. However, since impact failure happens at 470 MPa for this material, we need to increase the thickness from 1 mm to 2.3 mm so that we can increase the speed from 4 km/h to 5 *km/h*. In terms of percentage, we must increase the thickness by 130% to get 25% speed increment. Clearly this is a high cost in terms of materials and weight. In view of the above, it is concluded that making the panel thicker is not an effective way to increase the merging speed. Therefore, an optimum thickness of 1 mm is used throughout this work.

3.2.2 Alternative body materials

Up to this point, all simulations have been done based on Steel 4340 as the sole material. Nonetheless, the use of alternative materials in vehicles is on the rise. The additional

materials that will be used in the simulations are listed in Table 1. The results of the simulations are shown in Figures 17 to 22. These results are based on 20° AI and 1 mm body panel thickness. The first alternative material to be investigated is AL 1060-H12, which is another metal alloy that has less strength than steel. For this material, the stress versus *IV* is shown in Figure 17, where the relationship is nonlinear proportional. Deformation of AL 1060-H12 panel versus IV is plotted in Figure 18. It is generally linearly proportional except for a small portion at low speed, where the effect is inverse. It could be due to the geometric design of the impacted area. The next material to be simulated is Composite, epoxy glass fiber. For this material, the stress versus *IV* is plotted in Figure 19. The plot exhibits a nonlinear relationship. The deformation of Composite, epoxy glass fiber versus *IV* is presented in Figure 20. The relationship is proportional and approximately linear. The third and final alternative material to be investigated is Plastic, ABS high impact. The stress versus *IV* for this material is plotted in Figure 21. It exhibits a nonlinear proportional relationship. Figure 22 shows the deformation versus *IV* for Plastic, ABS high impact. The plot exhibits a perfectly linear proportional relationship.

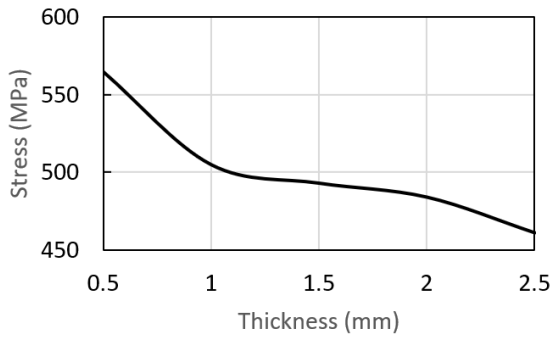

Figure 16. Stress vs. thickness for Steel 4340

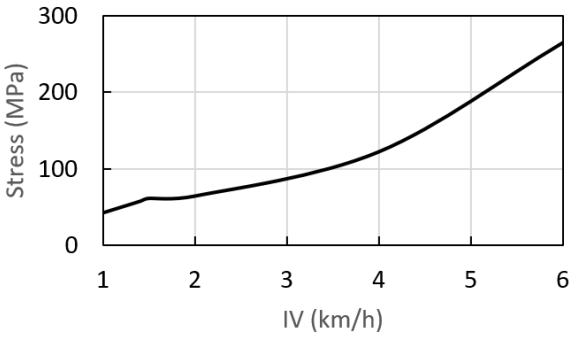

Figure 17. Stress vs. *IV* for AL 1060-H12

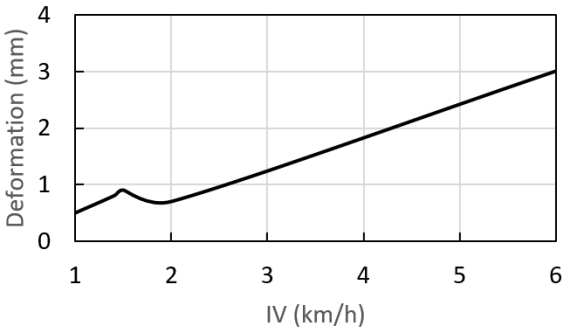

Figure 18. Deformation vs. *IV* for AL 1060-H12

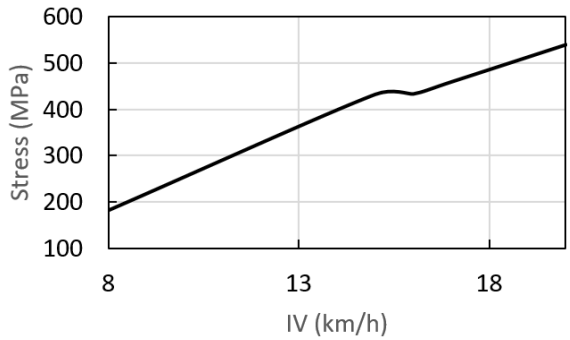

Figure 19. Stress vs. *IV* for Composite, epoxy glass fiber

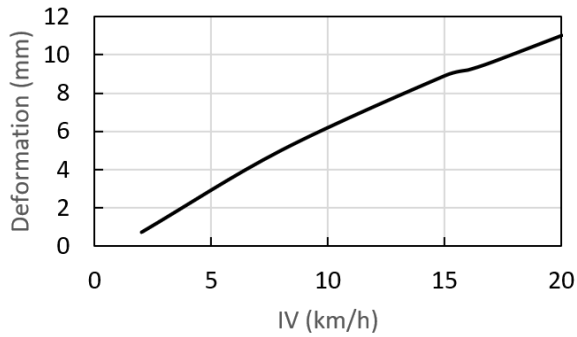

Figure 20. Deformation of Epoxy glass fiber

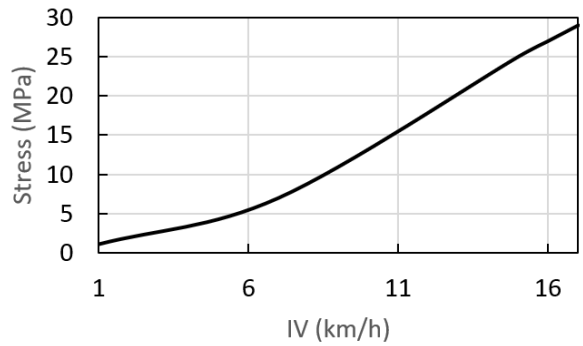

Figure 21. Stress of Plastic, ABS high impact

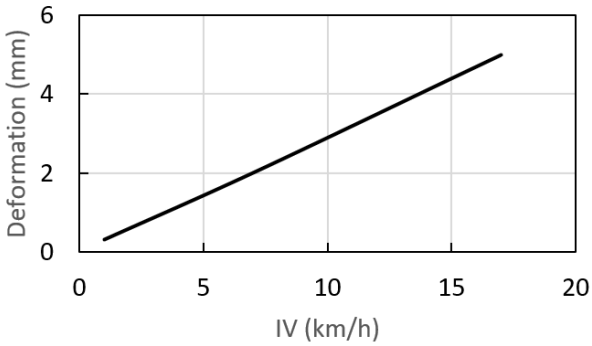

Figure 22. Deformation of Plastic, ABS high impact

As a result of the above simulations, the values of the safe docking velocities have been obtained for different conditions. The simulated scenarios include different angles of impact (AIs), parameters variation with time, behavior of kinetic energy and internal energy, history of impact response, deformation characteristics represented in stress-strain curve, effect of body panel thickness on the stress, and impact

response of different panel materials. The optimum docking velocities for different body panel materials are listed in Table 2; it is shown that the maximum safe docking velocity is 16 km/h. It can be achieved using Composite, Epoxy glass fiber or Plastic, ABS high impact. On the other hand, the lowest docking velocity is 1.4 km/h; it is obtained using AL 1060-H12 as the body panel material. It is worth noting that the velocities simulated in this work are relatively low; therefore, they do not represent typical crashes. Throughout this work, equivalent von-Mises stress have been used as the damage criterion. However, damage assessment can be based on another failure criterion, if warranted by the problem at hand. For the Composite, Epoxy glass fiber and Plastic, ABS high impact; specific damage criteria have been suggested; Hashin failure criteria [38] was proposed for Epoxy glass fiber composite; it states that the material is deemed damaged if exposed to *12 J* impact energy. This value corresponds to a speed of 4.7 *km/h*, as shown in Table 2. An alternative damage criterion was suggested for ABS high impact plastic [39]; it states that the material will suffer damage if exposed to 300 *G* acceleration. This amount corresponds to a velocity of 0.4 *km/h*, which is very low, as compared to the value obtained based on von-Mises equivalent stress. The reason for this large difference could be due to differences in material composition, heat treatment, manufacturing method, or specific design of the simulated part. A dynamic finite element analysis conducted by Al-Huniti and Al-Habahbeh [40] showed that composite (cross-ply) pressure vessel has lower stress and higher deflection than the steel vessel, which agrees with the findings of this work.

Table 2. Optimum docking velocities for different materials

Material of body panel	Safe docking velocity (*km/h*) for the adopted failure criteria	
	von-Mises stress	Hashin & Gohel failure criteria
Steel 4340	4	---
AL 1060-H12	1.4	---
Composite-Epoxy glass fiber	16	4.7
Plastic-ABS high impact	16	0.4

4. CONCLUSIONS

This work introduces an innovative smart transportation system, which comprises a fleet of single-seat POD vehicles. It also investigates the safe methods for operating these vehicles. These PODs can join each other and form larger vehicles to meet passengers' demand. Afterwards, they can separate from each other based on customer request. The whole process will be automated and run efficiently using a central control room. Each POD can join other PODs from all sides using hitching ports located on its four sides. In this work, the process of joining two PODs in tandem configuration is investigated. As a result of this merger, a new vehicle will be formed which can accommodate two passengers.

By connecting the PODs, several benefits can be obtained; the first benefit is that after merging, the passengers can communicate directly and naturally. Secondly, if the road conditions allow it, one of the motors can be turned-off to save energy. Thirdly, the passengers will arrive at the destination simultaneously. Finally, no seat will be left vacant, which results in saving both energy and required road space.

However, during the merger of the two PODs, minor collisions may happen. The effects of these impacts are studied in this work and recommendations for safe docking speeds are presented. The theoretical basis of the numerical simulations are presented in terms of the constitutive equations. The simulations are performed using FEA tools where dynamic behavior of the two PODs during docking was investigated.

The results showed that the two PODs can merge together safely without inducing any damage. However, if the merging process was not aligned perfectly, the merging speed should be reduced so as to control the resulting stresses. These speeds are obtained and presented in Table 2 for different body panel materials. The results of this work can help to develop a demand-based autonomous transportation system that is adaptable and flexible. It is noted that the resulting docking speeds are highly dependent on the type of material as well as the type of damage criterion used. It is further noted that nonmetallic materials have higher tolerance than metallic materials in response to docking impact. On the other hand, increasing the thickness of the body panel had little effect on the impact resistance. The obtained docking speeds were between 1.4 and 16 km/h, depending on the POD material. It is noted that the variation of the docking speeds is large. This means the merging process can be controlled using different combinations of materials and design configurations. As a recommendation for future work, alternative set of POD designs can be investigated, as well as their merging scenarios, materials and configurations. In addition, if physical prototypes are made, the docking process should be tested and confirmed to be safe at recommended speeds.

REFERENCES

[1] Priev, A. (2021). Vehicles for variably sized transportation. US Patent for Vehicles for variably sized transportation Patent, Patent # 10,882,575. https://patents.justia.com/patent/10882575.

[2] Williams, P.R., Kessler, P., Herold, L. (2019). Transportation system. US Patent 10359783B2. https://patents.google.com/patent/US6810817B1/en.

[3] Anschuber, S., Stempfer, G. (2016). Method for operating a vehicle combination, vehicle combination, towing vehicle, and work device. US Patent Application for Method for Operating a Vehicle Combination, Vehicle Combination, Towing Vehicle, and Work Device Patent Application (Application #20180134300). https://patents.justia.com/patent/20180134300.

[4] Han, J.W., Kwak, S.Y., Ham, H.S., Ha, J.S. (2018). Electronic docking vehicle. US Patent 9,914,495. https://patents.justia.com/ patent/9914495.

[5] Evans. (2018). Intelligent POD management and transport. US Patent 10,150,524. https://patents.justia.com/patent/10759286.

[6] Cervantes, V., Laborde, J. (2020). U.S. Patent No. 10,538,240. Washington, DC: U.S. Patent and Trademark Office. https://patents.google.com/patent/US20150269845.

[7] Wright. (2019). Self-powered actively steerable converter dollies for long combination vehicles. US Patent 10,518,831, https://uspto.report/company/Wrightspeed-Inc/patents.

[8] Zong, F., Wang, M., Tang, J., Zeng, M. (2022). Modeling AVs & RVs' car-following behavior by considering impacts of multiple surrounding vehicles and driving characteristics. Physica A: Statistical Mechanics and Its Applications, 5891: 126625. https://doi.org/10.1016/j.physa.2021.126625

[9] Xia, H., Chen, J., Liu, Z., Lan, F. (2020). Coordinated motion control for automated vehicles considering steering and driving force saturations. Transactions of the Institute of Measurement and Control, 42(1): 157-166. https://doi.org/10.1177/0142331219879342

[10] Walker, C.L., Boyce, B., Albrecht, C.P., Siems-Anderson, A. (2020). Will weather dampen self-driving vehicles? Bulletin of the American Meteorological Society, 101(11): E1914-E1923. https://doi.org/10.1175/BAMS-D-19-0035.1

[11] Chen, H., Zhou, R., Liu, Z., Sun, X. (2021). Exploring the mechanism of crashes with autonomous vehicles using machine learning. Mathematical Problems in Engineering, 5524356. https://doi.org/10.1155/2021/5524356

[12] Malik, S., Bandi, P., Sun, W. (2021). An experimental study of denial of service attack against platoon of smart vehicles. 4th International Conference on Connected and Autonomous Driving, MetroCAD, Detroit, MI, USA, pp. 23-30. https://ieeexplore.ieee.org/document/9499332.

[13] Chen, Q., Xie, Y., Ao, Y., Li, T., Chen, G., Ren, S., Wang, C., Li, S. (2021). A deep neural network inverse solution to recover pre-crash impact data of car collisions. Transportation Research Part C: Emerging Technologies, 126: 103009. https://doi.org/10.1016/j.trc.2021.103009

[14] Tho, Q.H., Phap, H.C., Phuong, P.A. (2022). Motion planning solution with constraints based on minimum distance model for lane change problem of autonomous vehicles. Mathematical Modelling of Engineering Problems, 9(1): 251-260. https://doi.org/10.18280/mmep.090131

[15] He, X., Liu, Y., Lv, C., Ji, X., Liu, Y. (2019). Emergency steering control of autonomous vehicle for collision avoidance and stabilization. Vehicle System Dynamics, 57(8): 1163-1187. https://doi.org/10.1080/00423114.2018.1537494

[16] Jin, X., Hou, H., Shen, M., Wu, H., Yang, K.H. (2018). Occupant kinematics and biomechanics with rotatable seat in autonomous vehicle collision: A preliminary concept and strategy. International Research Council on the Biomechanics of Injury, IRCOBI, Athens, Greece, pp. 106-113. http://www.ircobi.org/wordpress/downloads/irc18/pdf-files/17.pdf.

[17] Lee, K., Kum, D. (2019). Collision avoidance/mitigation system: Motion planning of autonomous vehicle via predictive occupancy map. IEEE Access, 7: 52846-52857. https://doi.org/10.1109/ACCESS.2019.2912067

[18] Corso, A., Du, P., Driggs-Campbell, K., Kochenderfer, M.J. (2019). Adaptive stress testing with reward augmentation for autonomous vehicle validation. IEEE Intelligent Transportation Systems Conference ITSC, 8917242: 163-168. https://doi.org/10.1109/ITSC.2019.8917242

[19] Xu, C., Ding, Z., Wang, C., Li, Z. (2019). Statistical analysis of the patterns and characteristics of connected and autonomous vehicle involved crashes. Journal of Safety Research, 71: 41-47. https://doi.org/10.1016/j.jsr.2019.09.001

[20] Dlugosch, M., Fritsch, J., Lukaszewicz, D., Hiermaier, S. (2017). Experimental investigation and evaluation of numerical modeling approaches for hybrid-FRP-steel sections under impact loading for the application in automotive crash-structures. Composite Structures, 174: 338-347. https://doi.org/10.1016/j.compstruct.2017.04.077

[21] Müller, U., Jost, T., Kurzböck, C., Stadlmann, A., Wagner, W., Kirschbichler, S., Baumann, G., Pramreiter, M., Feist, F. (2020). Crash simulation of wood and composite wood for future automotive engineering. Wood Material Science & Engineering, 15(5): 312-324. https://doi.org/10.1080/17480272.2019.1665581

[22] Yusof, N.S.B., Sapuan, S.M., Sultan, M.T.H., Jawaid, M. (2020). Conceptual design of oil palm fibre reinforced polymer hybrid composite automotive crash box using integrated approach. Journal of Central South University, 27(1): 64-75. https://doi.org/10.1007/s11771-020-4278-1

[23] Abdullah, N.A.Z., Sani, M.S.M., Salwani, M.S., Husain, N.A. (2020). A review on crashworthiness studies of crash box structure. Thin-Walled Structures, 153: 106795. https://doi.org/10.1016/j.tws.2020.106795

[24] Chen, Y., Cheng, X., Fu, K. (2020). Multi-material design of a vehicle body considering crashworthiness safety and social effects. International journal of crashworthiness, 25(5): 517-526. https://doi.org/10.1080/13588265.2019.16170-95

[25] Saenz-Dominguez, I., Tena, I., Esnaola, A., Sarrionandia, M., Torre, J., Aurrekoetxea, J. (2019). Design and characterisation of cellular composite structures for automotive crash-boxes manufactured by out of die ultraviolet cured pultrusion. Composites Part B: Engineering, 160: 217-224. https://doi.org/10.1016/j.compositesb.2018.10.046

[26] Liu, Q., Shen, H., Wu, Y., Xia, Z., Fang, J., Li, Q. (2018). Crash responses under multiple impacts and residual properties of CFRP and aluminum tubes. Composite Structures, 194: 87-103. https://doi.org/10.1016/j.compstruct.2018.04.001

[27] Öztürk, İ., Kaya, N., Öztürk, F. (2022). Effects of material failure criteria on design of vehicle parts under impact loading. International Journal of Crashworthiness, 27(1): 80-91. https://doi.org/10.1080/13588265.2020.1774480

[28] Song, Y., Chitturi, M.V., Noyce, D.A. (2021). Automated vehicle crash sequences: Patterns and potential uses in safety testing. Accident Analysis and Prevention, 153: 106017. https://doi.org/10.1016/j.aap.2021.106017

[29] Oztürk, I., Kaya, N., Oztürk, F. (2018). Design of vehicle parts under impact loading using a multi-objective design approach. Materials Testing, 60(5): 501-509. https://doi.org/10.3139/120.111174

[30] Yu, L., Gu, X., Qian, L., Jiang, P., Wang, W., Yu, M. (2021). Application of tailor rolled blanks in optimum design of pure electric vehicle crashworthiness and lightweight. Thin-Walled Structures, 161: 107410. https://doi.org/10.1016/j.tws.2020.107410

[31] Noorsumar, G., Rogovchenko, S., Robbersmyr, K.G., Vysochinskiy, D. (2021). Mathematical models for assessment of vehicle crashworthiness: A review. International Journal of Crashworthiness, https://doi.org/10.1080/13588265.2021.1929760

[32] Chombo, P.V., Laoonual, Y., Wongwises, S. (2021). Lessons from the electric vehicle crashworthiness leading to battery fire. Energies, 14(16): 4802. https://doi.org/10.3390/en14164802
[33] Liu, X., Liang, R., Hu, Y., Tang, X., Bastien, C., Zhang, R. (2021). Collaborative optimization of vehicle crashworthiness under frontal impacts based on displacement oriented structure. International Journal of Automotive Technology, 22(5): 1319-1335. https://doi.org/10.1007/s12239-021-0115-2
[34] Gungor, O.E., She, R., Al-Qadi, I.L., Ouyang, Y. (2020). One for all: Decentralized optimization of lateral position of autonomous trucks in a platoon to improve roadway infrastructure sustainability. Transportation Research Part C: Emerging Technologies, 120: 102783. https://doi.org/10.1016/j.trc.2020.102783
[35] Al-Mamany, D.A., Zehawi, R.N., Hameed, A.H. (2022). High occupancy vehicle lane as per the buses flow rate and passenger trips. Periodicals of Engineering and Natural Sciences, 10(2): 74-79. http://dx.doi.org/10.21533/pen.v10i2.2797
[36] Ulrich, C., Friedrich, H.E., Weimer, J., Schmid, S.A. (2019). New operating strategies for an on-the-road modular, electric and autonomous vehicle concept in urban transportation. World Electric Vehicle Journal, 10. https://doi.org/10.3390/wevj10040091
[37] Hibbeler, R.C. (2016). Engineering mechanics-dynamics. 14th ed., Pearson Prentice Hall, New Jersey, USA. https://www.pearson.com/en-us/search.html?q=9780133976564.
[38] Nassir N.A., Gharkan, M.R. (2021). Impact response of composite laminates based on epoxy and glass fibre. 3rd International Conference on Materials Engineering & Science, Material Today: Proceedings, 42(5): 1901-1907. https://doi.org/10.1016/j.matpr.2020.12.229
[39] Gohel, G., Bhudolia, S.K., Elisetty, S.B.S., Leong, K.F., Gerard, P. (2021). Development and impact characterization of acrylic thermoplastic composite bicycle helmet shell with improved safety and performance. Composite Part B, 221. https://doi.org/10.1016/j.compositesb.2021.109008
[40] Al-Huniti, N., Al-Habahbeh, O.M. (2006). Composite LPG cylinders as an alternative to steel cylinders: Finite element approach. International Conference on Manufacturing and Material Processing (ICMM 2006), Kuala Lumpur, Malaysia, pp. 363-368. https://www.academia.edu/41966360.

NOMENCLATURE

POD_1	The first POD
POD_2	The second POD
PODs	Plural of POD
FEA	finite element analysis
CCR	central control room
AI	angle of impact
F_1	load on POD_1, kN
F_2	load on POD_2, kN
m_1	mass of POD_1, kg
m_2	mass of POD_2, kg
a_1	acceleration of POD_1, m/s^2
a_2	acceleration of POD_2, m/s^2
T_1	kinetic energy of POD_1, J
T_2	kinetic energy of POD_2, J
U	work done during impact, J
v_1	speed of POD_1, km/h
v_2	speed of POD_2, km/h
F	impact force, kN
A	affected area, m^2
IV	impact velocity, km/h
Y	yield strength, MPa

Greek symbols

σ	mechanical stress, MPa

Subscripts

i	initial state
f	final state